The quenching set of a MEMS capacitor in two-dimensional geometries

A. E. Lindsay

Department of Mathematics, University of Arizona, Tucson, Arizona, 85721, USA.
Present Address: Department of Mathematics and Maxwell Institute for Mathematical Sciences
Heriot-Watt University, Edinburgh, UK, EH14 4AS.

J. Lega

Department of Mathematics, University of Arizona, Tucson, Arizona, 85721, USA.

F. J. Sayas

Dept. of Mathematical Sciences, University of Delaware, 501 Ewing Hall, Newark, DE 19716, USA.

Abstract

The formation of finite time singularities in a nonlinear parabolic fourth order partial differential equation (PDE) is investigated for a variety of two-dimensional geometries. The PDE is a variant of a canonical model for Micro-Electro Mechanical systems (MEMS). The singularities are observed to form at specific points in the domain and correspond to solutions whose values remain finite but whose derivatives diverge as the finite time singularity is approached. This phenomenon is known as quenching. An asymptotic analysis reveals that the quenching set can be predicted by simple geometric considerations suggesting that the phenomenon described is generic to higher order parabolic equations which exhibit finite time singularity. These results suggest that MEMS devices could be constructed to perform exotic tasks.

Keywords: Finite time singularity, MEMS, Bi-Laplace Equations, Singular Perturbation Theory, Nanotechnology

1. Introduction

Micro-Electro Mechanical Systems (MEMS) are a combination of integrated circuits with moving elastic components built on a miniature scale. The micro-meter and nano-meter length-scales typical in the construction of MEMS necessitate the use of electrostatic forces for actuation. Advances in manufacturing processes have enabled MEMS practitioners to manipulate the interaction between elastic surfaces and electrostatic forces to fabricate a variety of complex devices with applications in every area of science and industry [1]. In such interactions, however, the elastic structures of the device can be overwhelmed if the

Email addresses: A.Lindsay@hw.ac.uk (A. E. Lindsay), lega@math.arizona.edu (J. Lega), fjsayas@math.udel.edu (F. J. Sayas)

electric forces acting on them are too strong. In such a case, an instability, called the *pull-in instability*, occurs. Modelling its consequences has been a topic of recent mathematical attention [13, 15, 16, 18, 19, 27, 20, 2, 4] and is also the purpose of this article.

In a capacitor type MEMS device, an elastic membrane is held fixed along its boundary above an inelastic substrate. When an electric potential V is applied between these surfaces, the upper elastic sheet deflects downwards towards the substrate. If V is small enough, the deflection will reach an equilibrium; however, if V exceeds the *pull-in voltage* V^*, no equilibrium configuration is attainable and the top plate will *touch down* on the substrate. Figure 1 shows a schematic representation of the device. A common model (*c.f.* [1, 3]) describing the behaviour of this device specifies that the dimensionless deflection $u(x,t)$ satisfies the parabolic fourth order partial differential equation

$$u_t = -\Delta^2 u + \delta\Delta u - \frac{\lambda}{(1+u)^2}, \qquad u(x,0) = 0, \quad x \in \Omega, \tag{1a}$$

together with the clamped boundary conditions

$$u = 0, \quad \partial_n u = 0, \quad x \in \partial\Omega. \tag{1b}$$

The PDE (1) was derived in [1] via a narrow gap limit by modelling the deflecting surface as a beam under tension being actuated by a Coulomb forcing term. The parameter δ quantifies the relative strength of tensile and flexural forces acting on the beam while λ represents the relative importance of electrostatic and elastic forces. Here Ω is a bounded region of $\mathbb{R}^2$, for example as shown in Fig.1. The existence of equilibrium solutions to equation (1a) with the Navier or *pinned* condition $u = \Delta u = 0$ on $\partial\Omega$ has been studied recently in [11, 12, 17]. Namely, it is known that under these boundary conditions there exists a λ^* such that whenever $\lambda > \lambda^*$, equation (1a) has no equilibrium solutions. For the clamped boundary condition (1b), much less is known about the loss of existence of equilibrium solutions in a general Ω.

In the present work, we restrict our attention to the fourth order MEMS problem

$$u_t = -\varepsilon^2\Delta^2 u - \frac{1}{(1+u)^2}, \qquad u(x,0) = 0, \quad x \in \Omega, \tag{2}$$

with boundary conditions (1b). The particular form of (2) is obtained from (1a) by neglecting the tension term Δu ($\delta = 0$), taking λt as a new time variable, and defining $\lambda = \varepsilon^{-2}$.

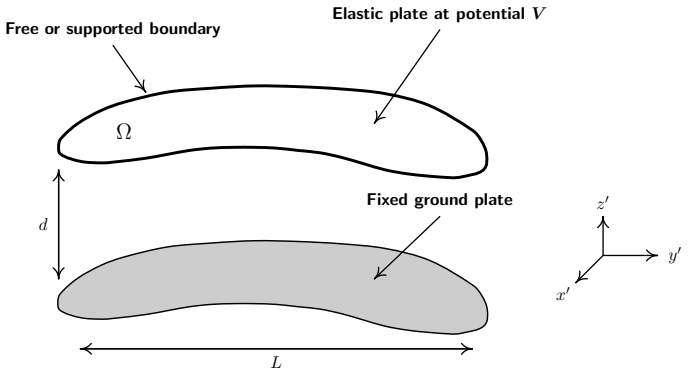

Figure 1: Schematic diagram of a MEMS capacitor (reproduced from [18]).

A recent study [13] considered the radially symmetric solutions of equation (2) in spatial dimensions 1 and 2. The existence of a critical value ε^* was established such that whenever $\varepsilon < \varepsilon^*$, the observed solution of (2) does not attain an equilibrium and consequently $u(x,t)$ takes on the value -1 in a finite time t_c. Correspondingly u_t becomes infinite in finite time - a phenomenon called *quenching*.

Further inspection of touchdown dynamics revealed the existence of a second threshold ε_c such that whenever $\varepsilon_c < \varepsilon < \varepsilon^*$, the location of touchdown is unique, but when $\varepsilon < \varepsilon_c$ and in the absence of external noise, touchdown can occur at multiple points in the domain. In the presence of noise, it is expected that one of these possible touchdown locations would be randomly selected by the dynamics. For example, when $\Omega = [-1,1]$ and $\varepsilon < \varepsilon_c \approx 0.066$, the surface described by the solution of (2) touches down at two points $x_c^{\pm}(\varepsilon)$ symmetric about the origin, while for $\Omega \equiv \{x \in \mathbb{R}^2, |x| \leq 1\}$ with $\varepsilon < \varepsilon_c \approx 0.0566$, radially symmetric solutions of (2) touch down on a ring of inner points with radius $r_c(\varepsilon)$. The singular perturbation analysis carried out in [13] provided the following predictions for $x_c^{\pm}(\varepsilon)$ and $r_c(\varepsilon)$ based on the touchdown time t_c:

$$x_c^{\pm}(\varepsilon) \sim \pm\Big[1 - \varepsilon^{\frac{1}{2}} f(t_c)^{\frac{1}{4}}[\eta_0 + f(t_c)\eta_1 + f^2(t_c)\eta_2]\Big], \qquad f(t) = 1 - (1-3t)^{\frac{1}{3}} \tag{3a}$$

$$r_c(\varepsilon) \sim 1 - \varepsilon^{\frac{1}{2}} f(t_c)^{\frac{1}{4}}\eta_0 - \varepsilon f(t_c)^{\frac{1}{2}}\eta_{\frac{1}{4}} - \varepsilon^{\frac{3}{2}} f(t_c)^{\frac{3}{4}}\eta_{\frac{1}{2}} + \cdots, \tag{3b}$$

where the values of the coefficients η_j in these expressions are determined quantities.

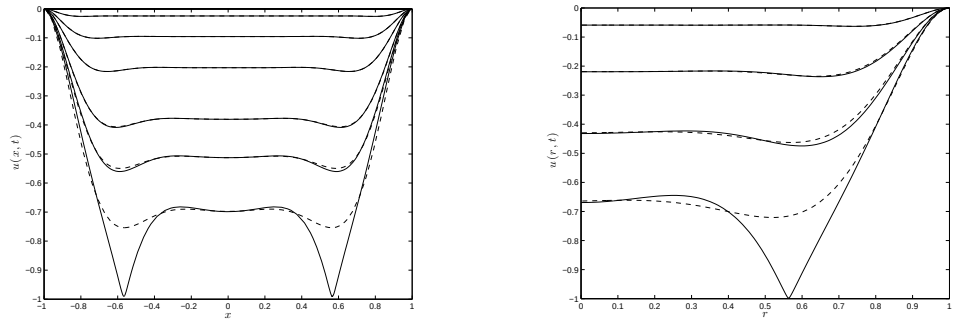

(a) Strip domain and $\varepsilon = 0.02$.

(b) Unit disc and $\varepsilon = 0.02$.

Figure 2: Full numerical (solid) and asymptotic (dashed) solutions of (2) for the strip (Panel (a)) and the unit disc under radially symmetric conditions (Panel (b)). The curves represent solutions for increasing times from top to bottom with the propagating boundary layer visibly moving inwards as time increases. [Panel (a) reproduced from [13]]

The singular perturbation analysis described above additionally reveals that the underlying cause of the multiple touchdown phenomenon is that the solution of (2) has a non-monotone profile in a stretching boundary layer in the vicinity of the boundary points, as illustrated in Fig. 2.

In the present work, we investigate the quenching set of equation (2) for a variety of bounded regions $\Omega \subset \mathbb{R}^2$ in the limit as $\varepsilon \to 0$. In this particular limit, the dynamics of the system may be approximated by a solution comprised of a flat central region interior to Ω coupled to a stretching boundary layer propagating normally from each boundary point toward the interior of Ω.

In the limit $\varepsilon \to 0$, an asymptotic analysis indicates that a point $x \in \Omega$ is a candidate for touchdown if there are multiple boundary points $y \in \partial\Omega$ for which the straight line between x and y meets $\partial\Omega$ normally at y. At such an interior point x, deformations due to the stretching boundary layer associated with each point y can meet constructively and make the solution near x enter the basin of attraction of a stable self-similar quenching solution (*c.f.* §5) more quickly. However, when ε is sufficiently small there is no opportunity for the boundary layers to interact constructively anywhere in Ω before touchdown, in which case the singular points are selected by a combination of second order effects and numerical noise, leading to symmetry breaking and/or instabilities. Consequently, the asymptotic predictions are shown to be very effective in several non-degenerate cases and moderately effective on some degenerate cases.

The outline of the paper is as follows. In §3, we construct a two term asymptotic solution to (2) in the limit $\varepsilon \to 0$ along the lines described previously. The validity of this asymptotic description is demonstrated for a variety of test regions Ω in §4. To obtain numerical solutions of (2) for a variety of regions, we use an adaptive finite element method with dynamic time-stepping close to touchdown. See supplemental material for a detailed description of the numerical algorithms. The leading order term of the expansion is shown to accurately predict the touchdown set for many non-degenerate regions, while in some degenerate examples the touchdown set is selected by effects that go beyond the leading order approximation and such considerations are included in our discussion. In §5 we analyze the local behaviour of solutions to (2) as the finite time singularity is approached. In §6 a summary of the main findings is presented along with a discussion of possible future work emanating from this study.

2. Numerics

Numerical simulations of equation (2) with boundary condition (1b) were performed in MATLAB, with a finite element method. The domain Ω is approximated by a mesh consisting of triangular cells, the size of which can be spatially adapted to maintain numerical accuracy in regions where touchdown occurs. This is done by means of a double simulation process. In the first simulation, an estimate of touchdown points is created. The grid is then refined several times around those points, using a newest-vertex-bisection rule on the set of elements that are close to the first estimates of touchdown points. The simulation is then run again on the refined grid. Time stepping is performed dynamically to guarantee accuracy close to touchdown.

We assume we have defined a triangulation $\mathcal{T}_h$ of a two-dimensional polygonal domain $\tilde{\Omega}$ that approximates Ω, in addition to the space V_h of $\mathbb{P}_1$ finite elements which vanish on $\partial\tilde{\Omega}$:

$$V_h = \{u_h \in \mathcal{C}(\Omega) \,:\, u_h|_{\partial\tilde{\Omega}} = 0, \quad u_h|_T \in \mathbb{P}_1 \,\forall T \in \mathcal{T}_h\},$$

where $\mathbb{P}_1$ is the set of bivariate linear polynomials. A basis of V_h is easily constructed by numbering the set of vertices of the triangulation $\{\mathbf{p}_1, \ldots, \mathbf{p}_J\}$ and considering the functions $\varphi_i \in V_h$ such that $\varphi_i(\mathbf{p}_j) = \delta_{ij}$. Associated to these functions, we can construct the stiffness matrix (which is the natural approximation of the $-\Delta$ operator with Dirichlet boundary conditions)

$$\mathbf{S}_{ij} = \int_\Omega \nabla\varphi_i \cdot \nabla\varphi_j$$

and the lumped mass matrix

$$\mathbf{M}_{ij} = \delta_{ij} \int_\Omega \varphi_i.$$

As an approximation of Δ^2, we will consider the matrix

$$\boldsymbol{\Delta}_2 := \mathbf{S}\mathbf{M}^{-1}\mathbf{S},$$

which is sparse, symmetric, positive definite and relatively easy to compute. This discretization is a slight variant of the bilaplacian approximation of Ciarlet and Raviart [7] (the original method uses the full mass matrix instead of its lumped approximation, making the matrix $\boldsymbol{\Delta}_2$ not directly computable). This method also appeared in [8] quoting [9] as the original source, but its approximation properties were only recently clarified in the very detailed analysis of [5].

To approximate $u(x,t)$, we first assume that we have constructed a sequence of time steps

$$0 = t_0 < t_1 < t_2 < \ldots t_n < \ldots$$

and we let $\delta_n := t_{n+1} - t_n$. We approximate $u(\cdot, t_n) \approx u_h^n \in V_h$ for all $n \geq 0$ and we identify u_h^n with its set of coefficients $\mathbf{u}^n := (u_1^n, \ldots, u_J^n)$ so that

$$u_h^n = \sum_{j=1}^{J} u_j^n \varphi_j \qquad u_j^n = u_h(\mathbf{p}_j, t_n) \approx u(\mathbf{p}_j, t_n).$$

Discretization of the parabolic equation

$$\partial_t u + \varepsilon^2 \Delta^2 u + \phi(u) = 0 \qquad \phi(u) := \frac{1}{(1+u)^2}$$

with homogeneous Dirichlet (clamped) boundary conditions

$$u|_{\partial\Omega} = \partial_n u|_{\partial\Omega} = 0 \qquad \forall t$$

is carried out using a Crank-Nicholson scheme for the linear part, a 2-step Adams-Bashforth scheme for the non-linear term, with lumped mass approximation of the identity operator in space and pointwise interpolation of the function ϕ. A time-step of the resulting method can be described as

$$\frac{1}{\delta_n}\mathbf{M}(\mathbf{u}^{n+1} - \mathbf{u}^n) + \frac{\varepsilon^2}{2}\boldsymbol{\Delta}_2(\mathbf{u}^{n+1} + \mathbf{u}^n) + (1+q_n)\mathbf{M}\boldsymbol{\phi}(\mathbf{u}^n) - q_n\mathbf{M}\boldsymbol{\phi}(\mathbf{u}^{n-1}) = \mathbf{0} \qquad n \geq 1,$$

where in this equation we have employed the notation

$$q_n = \frac{\delta_n}{2\delta_{n-1}} \qquad \boldsymbol{\phi}(\mathbf{v})_i = \phi(v_i).$$

Note that $\mathbf{M}$ is a diagonal matrix. Its effect on the time-stepping system can be understood as a rescaling of the equations to take into account the sizes of the elements around nodal points. A variational formulation of equation (2) would lead to a sparse non-diagonal mass matrix: the lumped mass version that we are using concentrates the values of the elements of the exact mass matrix in the diagonal, thus making its inversion straightforward. For the first time

step, we apply a simple predictor-corrector strategy, first using a Taylor approximation that is further corrected with a linearly implicit Crank-Nicolson step. Starting at $u(\cdot,0) \equiv 0$, since $\partial_t u(\cdot,0) \equiv -\phi(0) = -1$, the approximation $u(\cdot,t_1) \approx -\delta_0$ can be discretized by constructing the vector $\mathbf{u}_\circ^1 = -\delta_0(1,\ldots,1)$. This first guess is then corrected with

$$\frac{1}{\delta_0}\mathbf{M}\mathbf{u}^1 + \frac{\varepsilon^2}{2}\boldsymbol{\Delta}_2\mathbf{u}^1 + \frac{1}{2}\mathbf{M}(\boldsymbol{\phi}(\mathbf{u}_\circ^1) + \boldsymbol{\phi}(\mathbf{0})) = \mathbf{0}.$$

The matrices

$$\frac{\mathbf{M}}{\delta_n} + \frac{\varepsilon^2}{2}\boldsymbol{\Delta}_2$$

are sparse, symmetric, positive definite. The time-stepping strategy is complemented with a dynamic choice of the time step [28]. Given a starting parameter δ_τ, we construct

$$\delta_n := \delta_\tau g(\mathbf{u}^n), \qquad \text{where } g(\mathbf{v}) := \min_j |1+v_j|^3.$$

Note that this is the result of a forward Euler discretization at fixed time-step δ_τ of the equation

$$\frac{\mathrm{d}t}{\mathrm{d}\tau} = \min_{x\in\Omega} |1+u(x,t)|^3,$$

preceding the implicit time-stepping method for the associated PDE. Integration is carried out until

$$\min_j u_j^{n+1} < -1 + \delta_{\mathrm{tol}}$$

for a predetermined tolerance δ_{tol}.

3. Asymptotic description of small time solutions

If we assume that the one-dimensional features of solutions to (2) in small time and for small ε can be extended to the two-dimensional problem, we anticipate a solution $u(x,t)$ of (2) that is flat in the interior of Ω coupled to a boundary layer propagating inwards from the boundary $\partial\Omega$. The uniform interior solution is determined from (2) by neglecting the $\varepsilon^2\Delta^2 u$ term and considering the resulting problem:

$$\bar{u}_t = -\frac{1}{(1+\bar{u})^2}, \quad \bar{u}(0) = 0; \qquad \bar{u} = -1 + (1-3t)^{1/3}. \tag{4}$$

To analyze the propagating boundary layer, we first introduce an orthogonal coordinate system ρ, s, where $\rho > 0$ measures the distance from $x \in \Omega$ to $\partial\Omega$, whereas on $\partial\Omega$ the coordinate s denotes arc-length. In this co-ordinate system, (2) becomes

$$u_t = -\varepsilon^2\left(\partial_{\rho\rho} - \frac{\kappa}{1-\kappa\rho}\partial_\rho + \frac{1}{1-\kappa\rho}\partial_s\left(\frac{1}{1-\kappa\rho}\partial_s\right)\right)^2 u - \frac{1}{(1+u)^2}, \quad x\in\Omega; \tag{5a}$$

$$u = 0, \quad u_\rho = 0, \qquad \rho = 0, \tag{5b}$$

where $\kappa(s)$ is the curvature of $\partial\Omega$. The vicinity of the boundary is now rescaled with the variables

$$u(x,t) = f(t)\ v(z) \qquad z = \frac{\rho}{\phi(t;\varepsilon)}, \qquad \phi(t;\varepsilon) = \varepsilon^{1/2} f(t)^{1/4}, \qquad f(t) = 1-(1-3t)^{1/3}, \tag{6}$$

to arrive at

$$f_t \cdot \left(v - \frac{z}{4} v_z\right) = - \phi^4 \left(\frac{1}{\phi^2} \partial_{zz} - \frac{1}{\phi} \frac{\kappa}{1-\kappa\phi z} \partial_z + \frac{1}{1-\kappa\phi z} \partial_s \left(\frac{1}{1-\kappa\phi z} \partial_s \right) \right)^2 v - \frac{1}{(1+f\cdot v)^2}. \tag{7}$$

The expansion

$$v(z) = v_0(z) + \phi\, v_1(z) + \cdots \tag{8}$$

is substituted into (7) and terms equated to find at leading order that

$$v_{0zzzz} - \frac{z}{4} v_{0z} + v_0 = -1, \quad z > 0; \qquad v_0 = v_{0z} = 0, \quad z = 0; \quad v_0 \to -1, \quad z \to \infty. \tag{9}$$

This leading order solution is the same as in the one-dimensional case [13] and has no dependence on the curvature of the boundary; it depends only on the (perpendicular) distance from $\partial\Omega$. The profile $v_0(z)$ is numerically obtained by solving (9) on the finite interval $[0, L]$ with boundary conditions $v_{0z}(L) = v_{0zzz}(L) = 0$ for L sufficiently large to ensure convergence. The obtained profile is shown as a solid curve in Fig. 3.

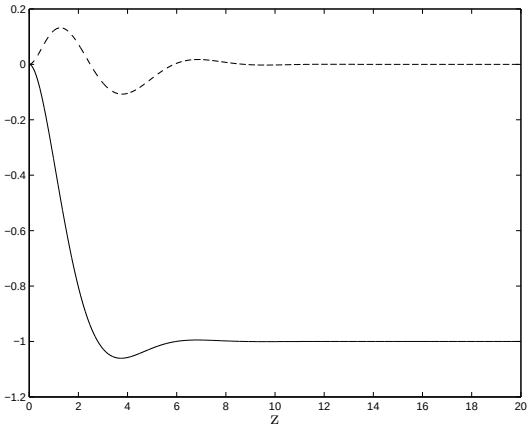

Figure 3: The profile $v_0(z)$, solution of (9) is displayed by the solid line, while $\bar{v}_1$, the solution of (11) is displayed by the dotted line.

At the next order we have the following problem, which involves the curvature $\kappa(s)$ of the boundary,

$$\begin{aligned} v_{1zzzz} - \frac{z}{4} v_{1z} + \frac{5}{4} v_1 &= 2\kappa(s) v_{0zzz}, \quad z > 0; \\ v_1 = v_{1z} = 0, \quad z = 0; &\qquad v_1 \to 0, \quad z \to \infty. \end{aligned} \tag{10}$$

Equation (10) is, as expected, consistent with the equation obtained in [13] for second-order corrections to the asymptotic profile of radially symmetric solutions on the unit disk. Its solution can be decomposed by writing $v_1 = \kappa(s)\bar{v}_1(z)$ where

$$\begin{aligned} \bar{v}_{1zzzz} - \frac{z}{4} \bar{v}_{1z} + \frac{5}{4} \bar{v}_1 &= 2 v_{0zzz}, \quad z > 0; \\ \bar{v}_1 = \bar{v}_{1z} = 0, \quad z = 0; &\qquad \bar{v}_1 \to 0, \quad z \to \infty. \end{aligned} \tag{11}$$

The solution of (11) is displayed (dashed curve) in Fig. 3.

The previous analysis indicates that the solution of (2), in the limit of small $\phi(t;\varepsilon) = \varepsilon^{1/2} f^{1/4}$, consists of a flat solution $\bar{u}(t)$ in the region interior to Ω, coupled to a boundary layer which extends inwards normally to the boundary $\partial\Omega$. Using this theory, we aim to predict the touchdown set for various two-dimensional domains. For certain geometries considered, the boundary admits the parametrization

$$\partial\Omega = \{(x_1, y_1) = (r(\theta)\cos\theta, r(\theta)\sin\theta) \mid 0 < \theta \leq 2\pi\}, \qquad r(\theta) = 1 + \delta\,\chi(\theta), \tag{12}$$

where $\chi(\theta)$ is a 2π periodic function. When δ is small, (12) describes a family of *almost circular* domains. To construct the solution to (2) at a point $x \in \Omega$, using the previous asymptotic formulation, it is first necessary to determine all boundary points $y \in \partial\Omega$ such that the straight line joining x and y meets the boundary orthogonally at y. The solution at $x \in \Omega$ is then constructed by linearly superimposing the expanding boundary layer solution described by (8) originating from each of these boundary points and then subtracting the far field behaviour. As an example, suppose for the point $x \in \Omega$ there are n boundary points $\{y_1, \ldots y_n\} \in \partial\Omega$ such that the straight line between x and y_i meets $\partial\Omega$ orthogonally at y_i, then the solution $u(x,t)$ is given by

$$u(x,t) \sim \bar{u}(t) + f(t)\left[\sum_{i=1}^{n} v_0\left(\frac{|x-y_i|}{\phi(t;\varepsilon)}\right) + \phi(t;\varepsilon)\,\kappa(\theta_i)\,\bar{v}_1\left(\frac{|x-y_i|}{\phi(t;\varepsilon)}\right) + 1\right], \quad \phi(t;\varepsilon) = \varepsilon^{\frac{1}{2}} f(t)^{\frac{1}{4}} \tag{13}$$

where $\theta_i = \arg(y_i)$ and for domains Ω with boundary (12),

$$\kappa(\theta) = \frac{r^2 + 2r_\theta^2 - r r_{\theta\theta}}{(r^2 + r_\theta^2)^{3/2}}.$$

3.1. Skeleton and touchdown set

From the considerations discussed in the previous section and the form of (13), it is clear that the distances $s_i = |x - y_i|$ play an important role in determining whether or not a given point $x \in \Omega$ will be a touchdown point. Indeed, based on the analysis of the one-dimensional problem [13] summarized previously, it is reasonable to assume that touchdown is more likely to occur on the set of points $x \in \Omega$ where boundary layer contributions minimize the value of u (*i.e.* make it closer to -1). In what follows, we use this assumption, together with the first order approximation (13), to predict the location of touchdown points for a wide range of domains Ω and then compare our predictions to the results of numerical simulations of (2). As a first approximation, we therefore define the set of possible touchdown locations as

$$\mathcal{T}_\Omega = \left\{ x \in \Omega \;\middle|\; s(x) = \eta_0\,\phi(t_c(\varepsilon);\varepsilon) \right\},$$

where $s(x) = d(x, \partial\Omega)$ denotes the shortest distance of $x \in \Omega$ to the boundary $\partial\Omega$, $\eta_0 \approx 3.7384$ is the global minimum of the profile $v_0(\eta)$, and $t_c(\varepsilon)$ is the touchdown time of (2). The asymptotic predictions formed in §3 suggest that points in $\mathcal{T}_\Omega$ that are equidistant from two or more boundary points y_i play a special role, since the terms in the sum of (13) constructively interact to lower the value of $u(x,t)$ at those points. Recall that the points $y_i \in \partial\Omega$ are such that the straight lines $l(x, y_i)$ through x and y_i intersect $\partial\Omega$ orthogonally.

Given a domain Ω, we therefore also define its *skeleton* $\mathcal{S}_\Omega$ as the set of points $x \in \Omega$ which are equidistant to two or more such boundary points y_i. In a more concise notation,

$$\mathcal{S}_\Omega = \left\{ x \in \Omega \;\middle|\; \exists y_1 \neq y_2 \in \partial\Omega,\ d(x,y_1) = d(x,y_2),\ l(x,y_1) \perp \partial_\tau(y_1),\ l(x,y_2) \perp \partial_\tau(y_2) \right\}. \tag{14}$$

Here $\partial_\tau(y)$ is a unit vector tangent to the boundary $\partial\Omega$ at $y \in \partial\Omega$. For small values of ε, small values of $s(x),\ x \in \mathcal{S}_\Omega$, are of interest. As explained previously, for touchdown to occur at $x \in \mathcal{S}_\Omega$, the quantity $s(x)$ should be such that $s(x) = \eta_0\,\phi(t_c(\varepsilon);\varepsilon)$, *i.e.* x should also belong to $\mathcal{T}_\Omega$.

As t increases, the boundary layer extends from $\partial\Omega$ toward the interior of Ω and the minimum of $u(x,t)$, as described by (13), decreases toward -1. The points where $u(x,t)$ attains its minimum value however depend on whether or not the boundary layer has already reached the skeleton $\mathcal{S}_\Omega$. Consequently, there is a crucial distinction to be made between the two cases $d(\mathcal{S},\partial\Omega) = 0$ and $d(\mathcal{S},\partial\Omega) > 0$. For a given value of ε and a given domain Ω, we define t_s as the smallest value of t for which there exists $x \in \mathcal{S}_\Omega$ such that $s(x) = \eta_0\,\phi(t;\varepsilon)$,

$$t_s = \min\left\{ t \;\middle|\; s(x) = \eta_0\,\phi(t;\varepsilon),\ x \in \mathcal{S}_\Omega \right\}.$$

This is the time at which the boundary layer that extends toward the interior of Ω first reaches $\mathcal{S}_\Omega$. If $t_s = 0$, then $d(\mathcal{S},\partial\Omega) = 0$ and we expect the touchdown points to be in $\mathcal{S}_\Omega$. However, if t_s is bounded away from 0, then for $t < t_s$, the first order solution v_0 leads to an approximation of $u(x,t)$ that reaches its minimum value on a closed curve $\omega(t)$, which is at the distance $\eta_0\,\phi(t;\varepsilon)$ from the boundary $\partial\Omega$. If touchdown occurs before $t = t_s$, i.e. if $t_c < t_s$, the touchdown points will be selected among points in $\omega(t_c)$ by the correction v_1 to v_0, which is curvature dependent. If on the other hand $t_s < t_c$, touchdown occurs after the boundary layer reaches $\mathcal{S}_\Omega$ and the first order approximation predicts that the touchdown points will be selected among those points in $\mathcal{S}_\Omega$ for which $s = \eta_0\,\phi(t_c(\varepsilon);\varepsilon)$. In other words, if we define τ_d as the touchdown set, we have

$$\tau_d(\Omega) = \begin{cases} \mathcal{T}_\Omega \cap \mathcal{S}_\Omega & \text{if } t_s \leq t_c \\ \mathcal{T}_\Omega \cap \mathcal{C}_\Omega & \text{if } t_s > t_c \end{cases},$$

where $\mathcal{C}_\Omega$ denotes the set of points in $\omega(t_c)$ that are favoured by curvature effects. Figure 4 illustrates how $\omega(t)$ and the skeleton $\mathcal{S}$ are defined.

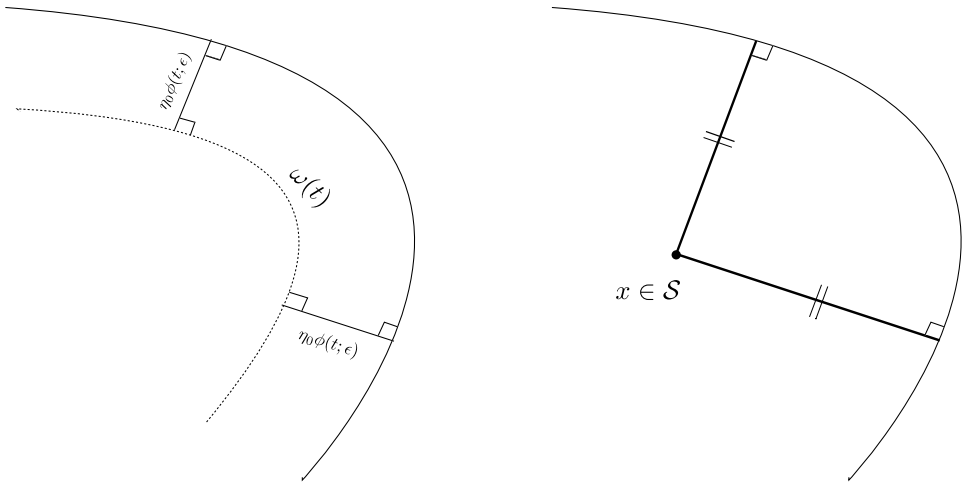

(a) $\omega(t)$ (b) $x \in \mathcal{S}$

Figure 4: The two structures, $\omega(t)$ and $\mathcal{S}$. (a) The set $\omega(t)$ consists of the points in Ω that are at the distance $\eta_0\,\phi(t;\varepsilon)$ from $\partial\Omega$. (b) The skeleton $\mathcal{S}$ is the set of points in Ω that are equidistant to two or more points on $\partial\Omega$ such that the line segments between x and those points meet $\partial\Omega$ orthogonally.

In all of the above situations, if the predicted touchdown set $\tau_d(\Omega)$ is degenerate, in the sense that symmetries of the domain Ω lead to a set $\tau_d(\Omega)$ that contains more than one point, randomness in the initial conditions or in the dynamics is expected to select one of the possible touchdown locations. In other words, we do not expect solutions that have the same symmetries as $\tau_d(\Omega)$ to be stable. Finally, since the above is based on a series of approximations, the actual touchdown location is expected to be in the vicinity of points in $\tau_d(\Omega)$. From a physical point of view, using an initial condition perturbed by small amplitude noise is an effort to mimic the inherent variability in the material properties of the deflecting surface and to understand the touchdown dynamics of (2) in its presence.

In what follows, we illustrate these ideas for various domains Ω. We first compare the predictions of the small-time asymptotic description with numerical simulations of (2) in the case of a semicircle of radius 1. In this situation, $t_s = 0$ and $\mathcal{S}_\Omega$ can be calculated analytically. The leading order asymptotic theory predicts that as ε is increased, the touchdown points lie on $\mathcal{S}_\Omega$ and satisfy $s(x) \simeq \eta_0\,\phi(t_c(\varepsilon);\varepsilon)$. Numerical results are in good agreement with this prediction, particularly when ε is small.

Next, the asymptotic theory of §3 is applied to the case where Ω is the disk of radius 1. For this example, $\mathcal{S}_\Omega$ consists of one point, the centre of the disk, and t_s is therefore bounded away from zero. As a consequence, we see that for $t < t_c < t_s$, the numerical solution is minimum on $\omega(t)$, which is a circle of approximate radius $r(t) = 1 - \eta_0\,\phi(t;\varepsilon)$. The touchdown set $\tau_d(\Omega)$ is equal to $\omega(t_c)$ since the curvature of the boundary is constant, and is therefore a circle of radius $r(t_c)$. Using an initial condition given by $u(x,0) = g_\eta(x)$ where g_η is a uniformly distributed random variable on $[-\eta, 0]$ with η small, we see that different realizations of $u(x,0)$ lead to different touchdown points on $\tau_d(\Omega)$. Moreover, we observe an instability of the radially symmetric solution in the azimuthal direction. More precisely, unstable modes, initially seeded by random initial conditions, grow exponentially in time, leading to an instability of the solution along $\omega(t)$. When the resulting changes in $u(x,t)$ are strong enough, nonlinearities come into play and locally drive the solution to touchdown.

Our third example is an ellipse. As for the disk, $t_s > 0$, but $\mathcal{S}_\Omega$ now consists of the section of the major axis of the ellipse between the two centres of curvature of its boundary. For $t_c < t_s$, touchdown occurs on the major axis as opposed to anywhere on $\omega(t_c)$ because of curvature effects. For $t_c > t_s$, touchdown occurs, with equal probability, at one of two points in $\mathcal{S}_\Omega$ symmetric with respect to the minor axis of the ellipse. In the absence of noise, touchdown would occur at these two points simultaneously.

The next example is the stadium, for which $\mathcal{S}_\Omega$ is a straight line joining the centres of the two semicircles that, together with a central rectangular region, form the domain Ω. This is an interesting example for two reasons: first, $\mathcal{S}_\Omega$ is "far away" from the boundary $\partial\Omega$ and as a consequence there is a reasonably large range of ε values for which $t_c < t_s$. In this case, the instability along $\omega(t)$ may lead to touchdown at any point along $\omega(t_c)$, depending on the intensity of the initial noise. However, for sufficiently small noise (or alternatively sufficiently large values of ε while the initial amount of noise is kept constant), it is observed that $\tau_d(\Omega)$ consists of two arcs in the interior of Ω, which can be numerically identified by running simulations of (2) with different noisy realizations of the initial conditions. Second, the curvature is discontinuous at the points of $\partial\Omega$ that connect the rectangular region of the stadium with the semicircles. We believe that, when the initial noise is small enough for this effect to be observed, it is this discontinuity in κ that determines the location of the endpoints of the two arcs that comprise $\tau_d(\Omega)$.

Our fifth example, a potato-shaped domain, allows us to test our theory on a domain Ω that does not have any particular symmetry. In this case, the skeleton is calculated numerically and we observe that touchdown occurs at one point, which moves along $\mathcal{S}_\Omega$ as ε varies. We conclude with a brief summary of our approach, which is illustrated on two other star-shaped domains, a gingerbread man and a square.

4. Application of the asymptotic theory

The theory developed in §3 is now demonstrated on a variety of test regions to illustrate its ability to predict qualitative and quantitative features of the touchdown set of (2).

4.1. Example 1: Semicircle

In the semi-circle case where $\Omega = \{(x_1, x_2) \in \mathbb{R}^2 \mid x_1^2 + x_2^2 \leq 1,\ x_2 \geq 0\}$, an analytical parameterization of the skeleton $\mathcal{S}$ is available. The simple geometric steps required to obtain $\mathcal{S}$ are displayed in Fig. 5(a), and lead to

$$\mathcal{S} = \left\{ \left(\frac{\cos\theta}{1+\sin\theta}, \frac{\sin\theta}{1+\sin\theta} \right) \,\middle|\, 0 < \theta < \pi \right\}. \tag{15}$$

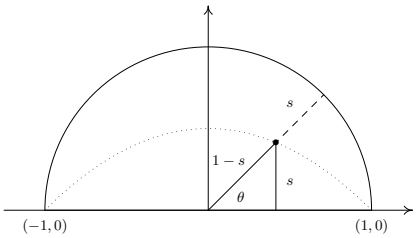

(a) Construction of $\mathcal{S}$ for semicircle.

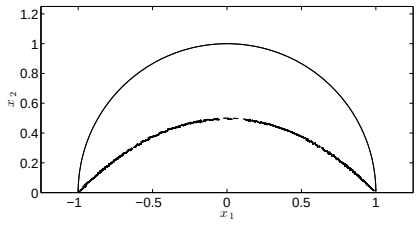

(b) Touchdown points coincide with $\mathcal{S}$.

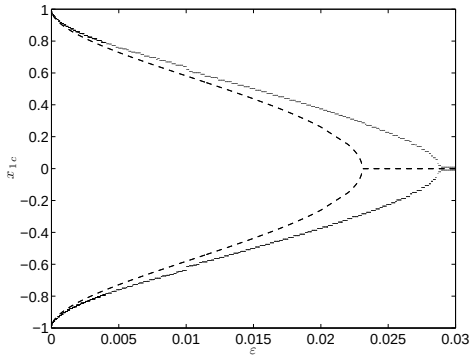

(c) Comparison of analytical and numerical touchdown point predictions.

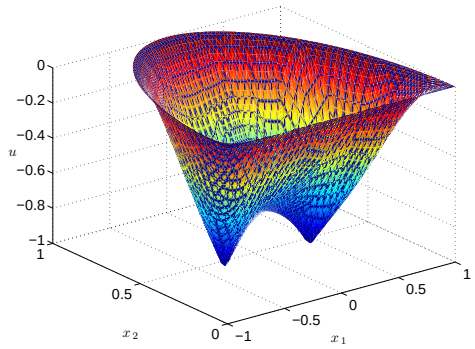

(d) Profile just before touchdown for $\varepsilon = 0.02$.

Figure 5: Panel (a) shows a schematic diagram indicating how to parameterize the skeleton $\mathcal{S}$ (dotted curve) of a semicircle. Panel (b) shows numerically obtained touchdown points for various values of ε (solid dots) lying directly on top of the skeleton $\mathcal{S}$ (dashed line). Panel (c) displays a comparison of numerical (solid dots) and asymptotic (dashed) predictions of the touchdown points location as ε varies. Panel (d) displays the solution profile just before touchdown ($\min_{x\in\Omega} u = -0.99$) for $\varepsilon = 0.02$.

In this example $t_s = 0$ and the leading order analysis of §3 predicts that touchdown only occurs on $\mathcal{S}$. In numerical experiments shown in Fig. 5(b), touchdown points (solid dots) are observed to lie on the skeleton (dashed curve), in agreement with the theory. The initial conditions were chosen to be $u = 0$ at $t = 0$ and the simulation was run for values of ε between 0.00001 and 0.03. For each value of ε the location of the global minimum in each half of the semi-circle was recorded along with an estimate for $t_c(\varepsilon)$ (details of how $t_c(\varepsilon)$ is estimated are given in §5).

The next test is to predict which point(s) of $\mathcal{S}$ are selected for touchdown for a given ε. For a fixed value of ε, an approximation for the touchdown set is formed by finding the points on $\mathcal{S}$ whose distance to the boundary is $s = \eta_0\phi(t_c(\varepsilon);\varepsilon)$, which corresponds to points where multiple depressions from the boundary meet constructively, as explained previously. A short calculation therefore provides the leading order prediction

$$x_{1c}^{\pm}(\varepsilon) = \begin{cases} \pm\sqrt{1-2\eta_0\phi_c(\varepsilon)}, & \eta_0\phi_c(\varepsilon) \le 1/2 \\ 0, & \eta_0\phi_c(\varepsilon) \ge 1/2 \end{cases}, \qquad \phi_c(\varepsilon) = \phi(t_c(\varepsilon);\varepsilon) \tag{16}$$

for the two touchdown points and also gives an estimate of ε_c, the threshold for multiple point touchdown as the implicit solution of $2\eta_0\phi_c(\varepsilon_c) = 1$. In Fig. 5(c), a comparison between the asymptotic prediction (16) and results of numerical simulations is displayed, which shows good agreement for small ε, but less favourable agreement when $\varepsilon \approx \varepsilon_c$. However, this is to be expected since when $\varepsilon \approx \varepsilon_c$, the touchdown points are very close together (see Fig. 5(d)),

and so the assumptions underpinning the asymptotic analysis leading to the prediction (16) are violated.

4.2. Example 2: Disk

For a disc of radius 1 centred at the origin, $\mathcal{S}_\Omega = \{(0,0)\}$ and so $t_s > 0$. The leading order theory predicts that touchdown should occur on $\omega(t_c(\varepsilon))$, which is a circle of radius $1 - \eta_0\phi(t_c(\varepsilon);\varepsilon)$. Indeed, experiments show that in the absence of initial noise, radially symmetric solutions of (2) touchdown simultaneously on all points of $\omega(t_c(\varepsilon))$ when $\varepsilon < \varepsilon_c$.

However, when non-radially symmetric solutions are considered the solution along $\omega(t)$ is not necessarily stable, and touchdown can therefore occur at one or more isolated points, should the radial symmetry be broken. Fig. 6(a) shows the profile close to touchdown for a simulation of (2) initialized with small random noise. This solution touches down at a single point. In Fig. 6(b), we show the touchdown locations (solid dots) for 100 realizations of (2) initialized with uniformly distributed random data on the interval $(-0.005, 0)$, for values $\varepsilon = 0.005, 0.015, 0.035$. The dashed curves indicate the set $\omega(t_c(\varepsilon))$ for the different values of ε, where in each case $t_c(\varepsilon)$ has been numerically obtained from the simulations of (2) with zero initial conditions in the absence of noise. In the presence of noise, touchdown therefore occurs at a single point of $\omega(t_c)$.

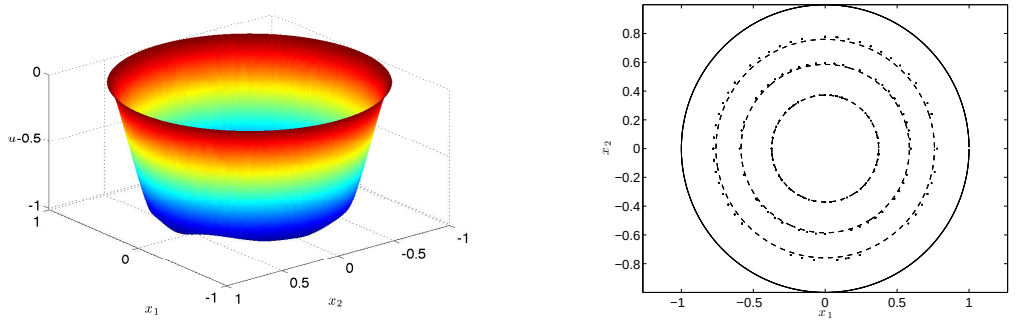

(a) Profile with single point touchdown, $\varepsilon = 0.01$.

(b) 100 realizations for each $\varepsilon = 0.005$, 0.015 and 0.035.

Figure 6: Left Panel: the profile close to touchdown on a disc is shown for a simulation of (2) initialized with small noise and $\varepsilon = 0.01$. Right panel: touchdown locations (small dots) for 100 realizations and $\varepsilon = 0.005, 0.015, 0.035$ are shown overlaid on $\omega(t_c(\varepsilon))$ (dashed lines).

4.2.1. Azimuthal instability along $\omega(t)$

The dependence of the solution u of (2) on the polar angle θ, along the ring $\omega(t)$ is now investigated. To do this, the numerical solution is interpolated onto a polar grid, which readily enables the temporal evolution of u on $\omega(t)$ to be followed. In Fig. 7, the deviation along $\omega(t)$ of the solution $u(r(t),\theta,t)$ from its average $\bar{u}(r(t),t)$ in the azimuthal direction, is displayed for the case $\varepsilon = 0.0037$ and small initial noise of amplitude 10^{-4}. Here, $r(t)$ is the radius of $\omega(t)$, numerically estimated as the distance from the origin of the point where u reaches its minimum value at time t.

The small scale noise of the initial condition is observed to be smoothed out by the initial dynamics of the system. However, some of the modes seeded by the noise grow exponentially,

indicating the presence of an instability in the θ direction. As $u(r(t),\theta,t)$ deforms in the azimuthal direction, nonlinear terms "pull down" the solution in those regions where $u(r(t),\theta,t)$ is closer to -1, thereby leading to touchdown at a single point along $\omega(t_c)$. Instabilities of line singularities have also been observed in rupture problems for thin film equations (*c.f.* [22]).

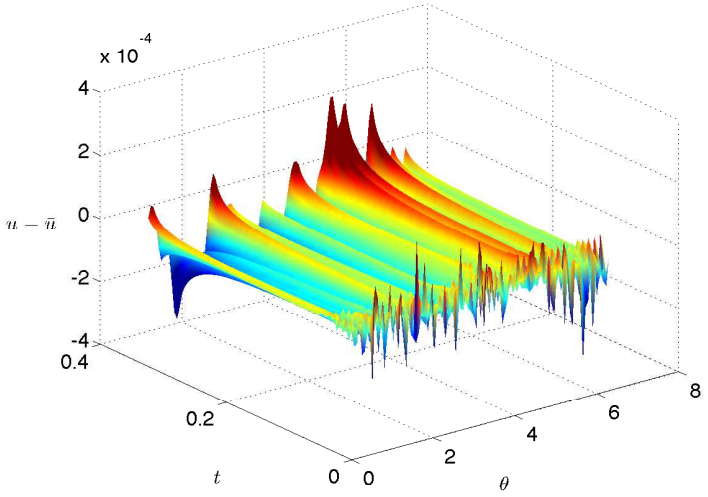

Figure 7: Plot of $u(r(t),\theta,t)-\bar{u}(r(t),t)$ as a function of time t and azimuthal variable θ, where $r(t)$ is the radius of $\omega(t)$ and the bar denotes average in θ. This figure illustrates the presence of an instability along $\omega(t)$, leading to a symmetry breaking of the solution in the azimuthal direction θ, and ultimately to touchdown at a single point on $\omega(t_c)$.

4.3. Example 3: Ellipse

The skeleton of an elliptical domain Ω of equation $\left(\frac{x_1}{a}\right)^2+\left(\frac{x_2}{b}\right)^2\le 1$, with $a>b$, may be found analytically as follows. The straight line between a point $x\in\mathbb{R}^2$ of coordinates (x_1,x_2) and a point on the boundary of Ω with coordinates $(a\cos\theta, b\sin\theta)$ is perpendicular to $\partial\Omega$ provided that

$$(b^2-a^2)\sin\theta\cos\theta+ax_1\sin\theta-bx_2\cos\theta=0,\qquad \theta\in[0,2\pi). \tag{17}$$

A point $x\in\Omega$ is in $\mathcal{S}_\Omega$ if there exists two distinct points $y_1=(a\cos\theta_1, b\sin\theta_1)$ and $y_2=(a\cos\theta_2, b\sin\theta_2)$ on the boundary of Ω that satisfy (17). Such a condition defines a linear system for x_1 and x_2, with determinant

$$\delta=ab\sin(\theta_2-\theta_1).$$

Since $\theta_1\neq\theta_2$, the determinant δ vanishes only when $|\theta_2-\theta_1|=\pi$. After substituting the condition $|\theta_2-\theta_1|=\pi$ into equation (17), it follows that

$$x_1=x_2=0,\qquad \theta_1\in\left\{-\frac{\pi}{2},0,\frac{\pi}{2},\pi\right\}. \tag{18}$$

For $\delta \neq 0$, the values of x_1 and x_2 are given by:

$$\begin{aligned} x_1 &= \frac{a^2-b^2}{b}\,\frac{\sin\theta_1\sin\theta_2\,(\cos\theta_2-\cos\theta_1)}{\sin(\theta_2-\theta_1)}, \\ x_2 &= \frac{a^2-b^2}{a}\,\frac{\cos\theta_1\cos\theta_2\,(\sin\theta_2-\sin\theta_1)}{\sin(\theta_2-\theta_1)}. \end{aligned} \tag{19}$$

When (19) is substituted into the condition $d(x,y_1) = d(x,y_2)$, we obtain

$$0 = (b^2-a^2)\,(\sin\theta_1-\sin\theta_2)\left(\sin\theta_1+\sin\theta_2+2\frac{\cos(\theta_1-\theta_2)}{\sin(\theta_1-\theta_2)}\,(\cos\theta_1-\cos\theta_2)\right). \tag{20}$$

which is equivalent to either

$$x_1 = 0, \quad x_2 = \frac{b^2-a^2}{b}\sin\theta_1, \qquad \theta_2 = \pi-\theta_1; \tag{21}$$

$$x_1 = \frac{a^2-b^2}{a}\cos\theta_1, \quad x_2 = 0, \qquad \theta_2 = -\theta_1. \tag{22}$$

Points x whose coordinates are given by (18) are such that $d \equiv d(x,y_1) = d(x,y_2)$ satisfies $d = a$ or $d = b$. Points x satisfying (21) are such that

$$d^2 = a^2\left(1-\sin^2\theta_1\left(1-\frac{a^2}{b^2}\right)\right), \tag{23}$$

which implies $a \leq d \leq a\frac{a}{b}$. Finally, points x whose coordinates satisfy (22) are such that

$$d^2 = b^2\left(1-\cos^2\theta_1\left(1-\frac{b^2}{a^2}\right)\right), \tag{24}$$

which implies $b\frac{b}{a} \leq d \leq b$. A comparison of expressions (23) and (24) reveals that under the assumption $a > b$, the skeleton points of (22) correspond to values of d smaller than those of (21). The asymptotic theory of §3 can now be applied to predict the location(s) $x_c(\varepsilon)$ of touchdown by seeking points in the skeleton with $d = \eta_0\phi(t_c(\varepsilon),\varepsilon)$. Note that if $b\frac{b}{a} \leq \eta_0\phi(t_c(\varepsilon),\varepsilon) \leq b$, then touchdown is predicted to occur on the skeleton and equation (24) can be rearranged for $\cos\theta_1$ and $x_{1c}(\varepsilon)$ obtained from (21). If $\eta_0\phi(t_c(\varepsilon),\varepsilon) < b^2/a$, then touchdown is predicted to occur away from the skeleton and to leading order on $\omega(t_c(\varepsilon))$. However, the boundary of the domain attains its global maximum of curvature at points $(-a,0),(a,0)$ and so points along the major axis of the ellipse will receive a more negative contribution from terms in (13) and therefore touch down more quickly. In summary, a leading order approximation of the touchdown points based on the asymptotic theory of §3 is given by

$$x_{1c}^{\pm}(\varepsilon) = \begin{cases} \pm(a-\eta_0\phi_c), & \eta_0\phi_c \leq b^2/a; \\ \pm\sqrt{\left(\dfrac{a^2}{b^2}-1\right)(b^2-\eta_0^2\phi_c^2)}, & b^2/a \leq \eta_0\phi_c \leq b \\ 0, & b \leq \eta_0\phi_c \end{cases}; \qquad x_{2c}^{\pm}(\varepsilon) = 0. \tag{25}$$

In (25), the expression for $x_{1c}^{\pm}(\varepsilon)$ is a piecewise continuous function of ε and $\phi_c = \phi(t_c(\varepsilon), \varepsilon)$. Figure 8 shows simulated profiles with touchdown on $\omega(t_c(\varepsilon))$ and $\mathcal{S}$, as well as the skeleton $\mathcal{S}$. The bottom right panel shows a comparison between numerically observed touchdown locations and the predictions of the leading order theory. As expected, the agreement is very good for small values of ε.

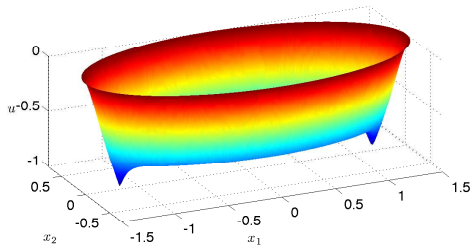

(a) Profile close to touchdown, $\varepsilon = 0.01$

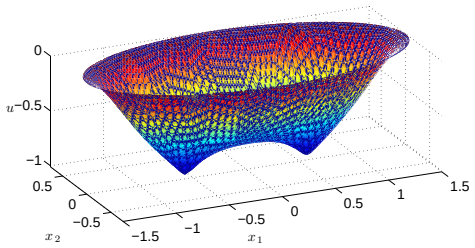

(b) Profile close to touchdown, $\varepsilon = 0.05$

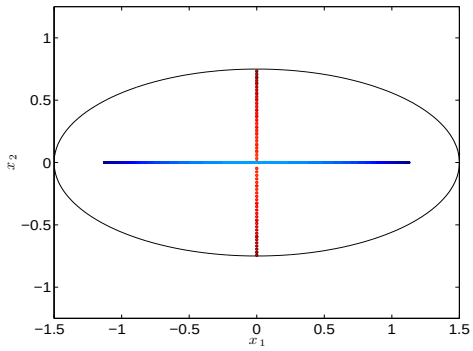

(c) Domain with $\mathcal{S}$

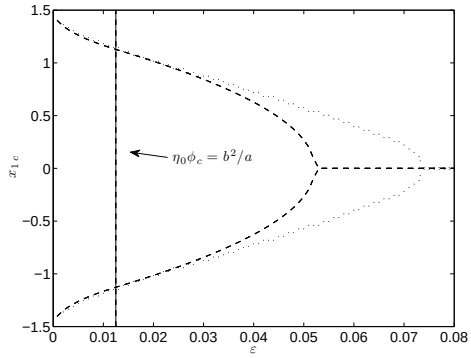

(d) Comparison of analytical (dashed) and numerical (solid dots) touchdown points.

Figure 8: Panels (a) and (b) show touchdown away from and on $\mathcal{S}$ respectively, in the case of an elliptical domain. The profiles shown are for $\varepsilon = 0.01$ and $\varepsilon = 0.05$ respectively and correspond to $\min_{x\in\Omega} u = -0.99$. Panel (c) shows the skeleton $\mathcal{S}$ for the ellipse with the colouring of each $x \in \mathcal{S}$ indicating the distance to the closest contributing boundary points with red being larger and blue lower. Panel (d) shows a comparison of the analytical (dashed) prediction for $x_{1c}^{\pm}$ given by (25) and the numerically obtained touchdown points (dots). The vertical line indicates the border between touchdown away from and on $\mathcal{S}$.

4.4. Example 4: Stadium

The stadium domain considered in this example is the interior of the region formed by joining two semicircles of unit radius on either end of a rectangle with side-lengths 1 and 1.5. The skeleton of this domain consists of the line segment along the y-axis joining the centres of the two semicircles. With our choice of coordinates, the end points of $\mathcal{S}$ have coordinates $(0, 0)$ and $(1.5, 0)$ (see dashed curve of Fig. 9). In this case $t_s > 0$, and so for $t_c(\varepsilon) < t_s$, the asymptotic theory developed in §3 predicts touchdown on the set $\omega(t_c(\varepsilon))$. For the stadium, this set has the shape of a smaller stadium, located at a distance $\eta_0\phi(t_c(\varepsilon), \varepsilon)$ from the boundary $\partial\Omega$. However, numerical simulations initiated with zero initial conditions and ε small enough so that $t_c(\varepsilon) < t_s$, indicate touchdown at two isolated points along the horizontal axis, as opposed to anywhere on $\omega(t_c(\varepsilon))$.

This example is therefore interesting because the asymptotic theory of §3 does not capture the touchdown properties of (2) due to a combination of factors not included in the leading order theory. In the presence of initial noise, the touchdown location is expected to be selected as the result of a competition between the instability along $\omega(t)$ (as in the disc case) and higher order effects. For initial noise of sufficiently strong magnitude, touchdown should thus be able to occur anywhere on $\omega(t_c(\varepsilon))$. This is illustrated in Fig. 9, in which the touchdown location is shown for the results of several hundred simulations of (2), for five different values of ε. In each case, the value of ε is such that $t_c(\varepsilon) < t_s$, and touchdown is recorded at a single point only. We see that for the smallest value of ε (outer curve), the 200 realizations of (2) initialized with random data allow us to recover most of $\omega(t_c(\varepsilon))$. Due to corrections that depend on curvature, touchdown is however more likely to occur on the semicircular sections of $\omega(t_c(\varepsilon))$. Figure 9 confirms this expectation, but also shows that for larger values of ε, points on the semicircular sections of $\omega(t_c(\varepsilon))$ that are closer to the stadium axis appear to be preferred touchdown locations. We believe that this is a consequence of the discontinuity in curvature at those points of $\partial\Omega$ where the rectilinear and semicircular sections of the domain boundary meet; as the effect of the noise diminishes (*i.e.* as ε increases), the touchdown set depends more strongly on curvature effects and becomes confined to two arcs of a circle.

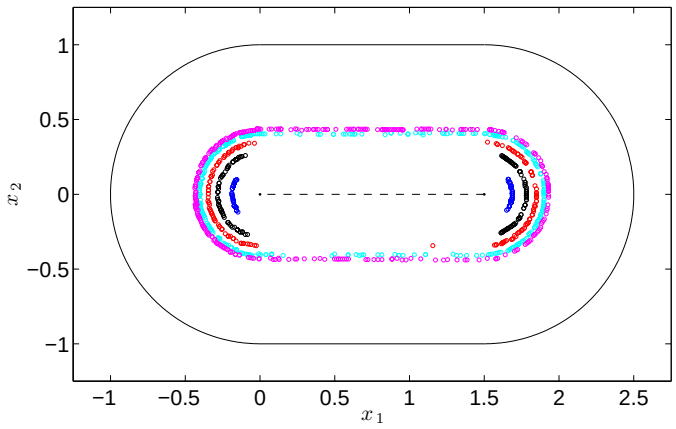

Figure 9: Solid dots represent touchdown points inside the stadium for various values of ε. From inside out, $\varepsilon = 0.01,\ 0.005,\ 0.0025,\ 0.001,\ 0.0005$. The magnitude of the initial noise (10^{-4}) is the same for all realizations of initial conditions and all values of ε.

4.5. Example 5: Potato

In this example, the touchdown set is investigated for a domain with no symmetries. The domain is the region interior to the parameterized boundary

$$\partial\Omega = \{(x_1, y_1) = (r(\theta)\cos\theta, r(\theta)\sin\theta) \mid 0 < \theta \leq 2\pi\}, \qquad r = 1 + 0.3\ (\cos\theta + \sin 2\theta). \quad (26)$$

We whimsically refer to this domain as *the potato* due to its appearance which is displayed in Fig. 10(a), along with its numerically obtained skeleton, $\mathcal{S}$. The colouring of $x \in \mathcal{S}$ in Fig. 10(a) indicates the distance to the nearest boundary points which contribute to $x \in \mathcal{S}$ with red being larger and blue lower (*c.f.* (14) for the definition of boundary contributions). According to the asymptotic theory of §3, touchdown should occur at the point of largest curvature on $\omega(t_c(\varepsilon))$ for small values of ε, and on $\mathcal{S}$ when ε is such that $t_c(\varepsilon) > t_s$. This is

confirmed by the simulations of Fig. 10(b), which show the touchdown points observed for a range of ε values between 0.0025 and 0.150, with zero (and thus noiseless) initial conditions. For $t_c(\varepsilon) > t_s$, the touchdown location on $\mathcal{S}$ jumps from the left side of $\mathcal{S}$ to its right side as ε increases above a critical value numerically estimated at $\varepsilon_p \approx 0.04855$. Why this happens may be understood from the simulations of Fig. 11(a-c), which show the solution $u(x_1, x_2, t)$ near touchdown for values of ε below, near, and above ε_p respectively. In all cases, the profile of u has two minima, but their relative depths depend on ε, so that touchdown occurs at the location of the left minimum for $\varepsilon < \varepsilon_p$ and at the location of the right minimum for $\varepsilon > \varepsilon_p$. When $\varepsilon = \varepsilon_p$, touchdown can occur simultaneously at two points in the absence of noise as suggested by Fig. 11(b).

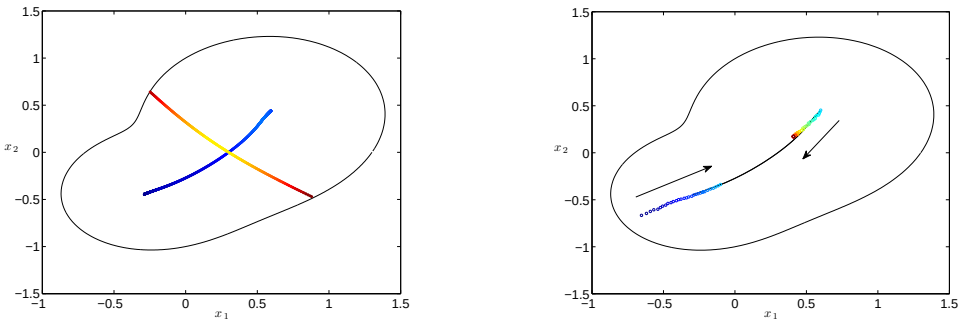

(a) Domain with Full Skeleton

(b) Touchdown points with partial skeleton.

Figure 10: Panel (a): Numerically obtained skeleton for the potato domain with blue indicating small and red larger distances. Panel (b): numerically obtained touchdown set indicated with coloured dots where blue corresponds to small and red large values of ε. The arrows point in the direction of increasing ε values. For comparison, the portion of $\mathcal{S}$ associated with smaller values of $s = d(x, \partial\Omega)$ is shown as a solid black line.

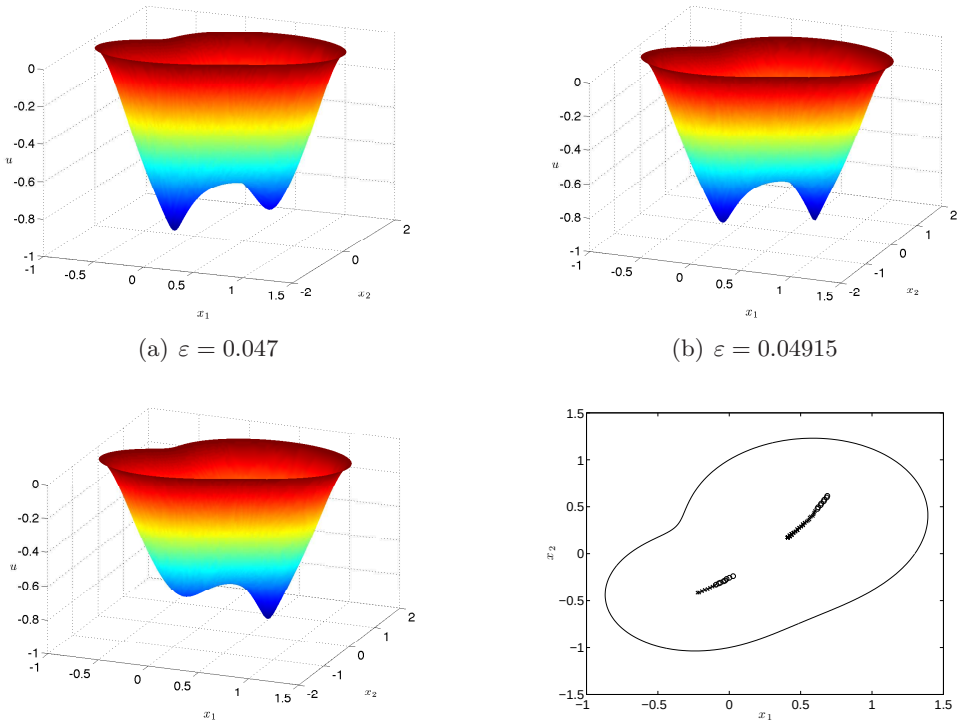

(a) $\varepsilon = 0.047$

(b) $\varepsilon = 0.04915$

(c) $\varepsilon = 0.055$

(d) Minima of u and touchdown location

Figure 11: Panels (a)-(c) show the profile of u for ε below, near, and above $\varepsilon_p \approx 0.04855$, respectively. Panel (d) shows the location of the two minima of u, the touchdown point being marked with a cross and the other minimum with a circle.

4.6. Summary

In this section, we summarize our approach to predict the touchdown set of (2) for general, star-shaped geometries. To infer the touchdown set from the asymptotic theory of §3, the first step is to construct the skeleton $\mathcal{S}$ for the domain Ω. If $\mathcal{S}$ touches $\partial\Omega$, $t_s = 0$; if not, $t_s > 0$. In the latter case, we predict touchdown on $\omega(t_c(\varepsilon))$ for $t_c(\varepsilon) < t_s$ and on $\mathcal{S}$ when $t_c(\varepsilon) > t_s$.

When $t_c(\varepsilon) < t_s$, touchdown typically occurs at a single point on $\omega(t_c)$, selected by curvature effects as well as by any long-range instability that can break the translational symmetry along $\omega(t)$. When $t_c(\varepsilon) > t_s$, touchdown occurs on $\mathcal{S}$.

If $\mathcal{S}$ is invariant under some symmetry, the possible touchdown set is typically a collection of points also invariant under that same symmetry. Touchdown generically occurs at one of these points, selected by randomness in the initial conditions or numerical noise. In the absence of symmetry breaking effects however, touchdown could occur simultaneously at all of the points in the touchdown set. As an example, we consider the gingerbread man domain Ω defined as the region enclosed by the curve

$$\partial\Omega = \{(x_1, y_1) = (r(\theta)\cos\theta, r(\theta)\sin\theta) \mid 0 < \theta \leq 2\pi\}, \qquad r(\theta) = 1 + 0.2\cos 5\theta. \tag{27}$$

The partial skeleton, such that $s = d(x, \partial\Omega) < 0.8$, is displayed in Fig. 12(a). We see that the portion of $\mathcal{S}$ corresponding to small s values does not touch $\partial\Omega$ and that $\mathcal{S}$ has, as expected,

a fivefold symmetry. In the absence of noise and with ε large enough for touchdown to occur on $\mathcal{S}$, touchdown may occur at five points simultaneously, provided the numerical grid has the same symmetry as Ω. This is illustrated in Fig. 12(b), which shows the solution of (2) for $\varepsilon = 0.02$ and $\inf_{x\in\Omega} u(x,t) = -0.99$.

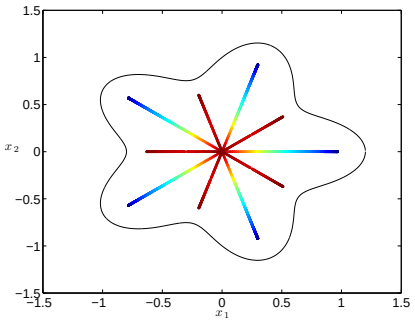

(a) Partial skeleton, $s < 0.8$.

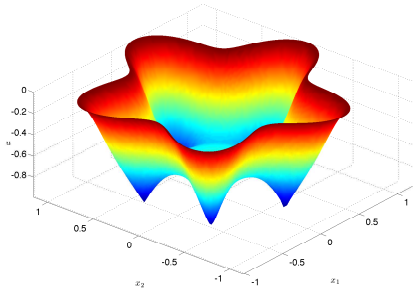

(b) Solution close to touchdown, $\varepsilon = 0.02$.

Figure 12: The left figure displays the partial skeleton for the gingerbread man for values $d(x, \partial\Omega) := s < 0.8$. Blue colours indicate smaller values of s while red indicating larger. The right panel shows the solution of (2) close ($\inf_{x\in\Omega} u(x,t) = -0.99$) to touchdown for $\varepsilon = 0.02$. In the absence of noise, touchdown occurs at five distinct points on $\mathcal{S}$.

If on the other hand $t_s = 0$, touchdown always occurs on $\mathcal{S}$. As an example, we consider the square region $\Omega \equiv [-1,1] \times [-1,1]$. Its partial skeleton for $s < 1$ consists of its two diagonals and is shown in Fig. 13(a). If the numerics preserves the fourfold symmetry, we expect touchdown at four points along the diagonals of the square as demonstrated in Fig. 13(b). As the value of ε increases to ε_c, the four touchdown points merge at the origin.

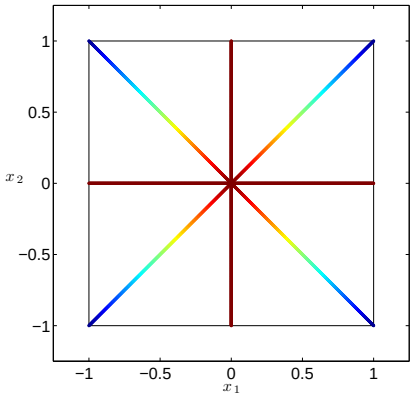

(a) Square skeleton.

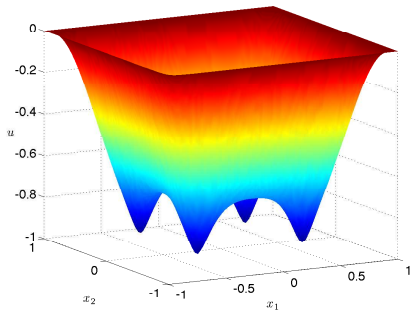

(b) Solution close to touchdown, $\varepsilon = 0.03$.

Figure 13: The left panel displays the skeleton for the square with blue colours indicating smaller values of s and red indicates larger. The right panel shows the solution of (2) close ($\inf_{x\in\Omega} u(x,t) = -0.99$) to touchdown. In the absence of noise, touchdown occurs at four distinct points along $\mathcal{S}$.

5. Local behaviour near touchdown

We now turn to the asymptotic profile of the solution near touchdown. The discussion below follows that developed in [13] for touchdown at the origin, in the case of two-dimensional radially symmetric solutions. For more general treatments of singularity formation in higher order PDEs, the reader is referred to [21, 23, 24, 25, 26, 14] and the references therein.

We assume the solution u has a local self-similar profile of the form

$$u(x,t) = -1 + (t_c - t)^{1/3} v(\eta, s), \qquad \eta = \frac{x - x_c}{\varepsilon^{1/2}(t_c - t)^{1/4}}, \quad s = -\log|t_c - t| \tag{28}$$

near the touchdown point $x_c \in \mathbb{R}^2$. This assumption leads to an equation for $v(\eta, s)$, obtained by substituting (28) into (2). It reads

$$v_s = -\Delta_\eta^2 v - \frac{1}{4}\eta \cdot \nabla_\eta v + \frac{v}{3} - \frac{1}{v^2}, \qquad (s,\eta) \in \mathbb{R} \times \mathbb{R}^2. \tag{29}$$

Since quenching occurs locally near $x = x_c$, the solution may be expected to satisfy $u_t = \mathcal{O}(1)$ far from x_c, as $t \to t_c^-$. Since

$$u_t = (t_c - t)^{-2/3}\left[v_s + \frac{\eta}{4} v_\eta - \frac{v}{3}\right], \tag{30}$$

enforcing $u_t = \mathcal{O}(1)$ means that

$$v_s + \frac{\eta}{4} v_\eta - \frac{v}{3} = \mathcal{O}((t_c - t)^{2/3}), \qquad t \to t_c^-. \tag{31}$$

Since $|\eta| \to \infty$ as $t \to t_c^-$ for $x \neq x_c$, (31) provides a far field condition for (29). The similarity profile $v(\eta, s)$ is thus expected to solve

$$v_s = -\Delta_\eta^2 v - \frac{1}{4}\eta \cdot \nabla_\eta v + \frac{v}{3} - \frac{1}{v^2}, \qquad (s,\eta) \in \mathbb{R} \times \mathbb{R}^2; \tag{32a}$$

$$\nabla_\eta v = \nabla_\eta \Delta_\eta v = 0, \quad \eta = 0; \qquad v_s = \frac{v}{3} - \frac{\eta}{4} \cdot \nabla_\eta v, \quad |\eta| \to \infty. \tag{32b}$$

The touchdown profile of (2) as $t \to t_c^-$ is thus given by the solution of (32) in the limit $s \to \infty$ for fixed η. To investigate the existence of *self-similar* solutions, *i.e.* those satisfying $v_s \to 0$ as $s \to \infty$, we consider the problem

$$-\Delta_\eta^2 v - \frac{1}{4}\eta \cdot \nabla_\eta v + \frac{v}{3} - \frac{1}{v^2} = 0, \qquad \eta \in \mathbb{R}^2; \tag{33a}$$

$$\nabla_\eta v = \nabla_\eta \Delta_\eta v = 0, \quad \eta = 0; \qquad \frac{v}{3} - \frac{\eta}{4} \cdot \nabla_\eta v = 0, \quad |\eta| \to \infty. \tag{33b}$$

The existence and multiplicity of symmetric and asymmetric solutions to (33) is a challenging open problem. Additionally, the stability of any solutions to (33) under dynamics (32) must be addressed. Equations (32) and (33) are non-variational, non-constant coefficient, nonlinear PDEs and are accordingly challenging to study analytically. For these reasons we rely on numerical simulations to glimpse their solution properties. If one seeks a radially symmetric solution to (33) in terms of a single variable $r = |\eta|$, then we have the problem

$$-\left(v_{rrrr} + \frac{2}{r} v_{rrr} - \frac{1}{r^2} v_{rr} + \frac{1}{r^3} v_r\right) - \frac{r}{4}\, v_r + \frac{v}{3} - \frac{1}{v^2} = 0, \qquad r > 0, \tag{34a}$$

$$v_r = v_{rrr} = 0, \quad r = 0; \qquad \frac{v}{3} - \frac{r}{4} v_r = 0, \quad r \to \infty. \tag{34b}$$

The far field condition of (34b) generates the asymptotic behaviour $v \sim \alpha\, r^{4/3}$ as $r \to \infty$ where α is a nonlinear eigenvalue which is expected to take on a discrete number of values, each corresponding to a discrete solution of (34). After discretization of (34), Newton iterations are performed with initial guess

$$v_0(r;\alpha) = \sqrt[3]{\alpha^3 r^4 + 3}, \qquad \alpha > 0,$$

over a range of α. Convergence is observed to precisely two profiles $\bar{v}_1(r)$ and $\bar{v}_2(r)$ with corresponding values of α, $\alpha_1 = 0.7265$ and $\alpha_2 = 0.0966$. The numerical investigation of the stability of these solutions was performed in [13], where it was shown that only $\bar{v}_1(r)$, shown as a dashed curve in Fig. 14(d), is dynamically stable. It is therefore expected that if the touchdown profile is self-similar, it should locally be given by the solution $\bar{v}_1(r)$. We remark that the existence of precisely two self-similar profiles has been observed (*c.f.* [25, 14]) in related higher order finite time singularity problems.

We now numerically investigate the validity of this assumption in the case of touchdown in an elliptical domain given by

$$\left(\frac{x_1}{a}\right)^2 + \left(\frac{x_2}{b}\right)^2 \leq 1; \qquad a = 1.5, \quad b = 0.75.$$

Note that this elliptical region is the same considered in §4.3. For our comparison, the value $\varepsilon = 0.05$ is used and the solution of (2) is numerically advanced until $\min_{x\in\Omega} u(x,t) = -0.999$. From equation (28), we expect the touchdown profile to satisfy the asymptotic relationship

$$\min_{x\in\Omega}(1 + u(x,t))^3 \propto (t_c - t) \tag{35}$$

as $t \to t_c^-$. As a consequence, the touchdown time t_c can be accurately estimated by finding the intercept of a linear fit between $\min_{x\in\Omega}(1 + u(x,t))^3$ and t with the horizontal axis. Indeed, this linear fit is found to be very good with a residual value of $r = -0.999998$ and a resulting touchdown time of $t_c = 0.311028113536382$. This good agreement suggests that there are no logarithmic corrections to the quenching rate in this problem, however, such corrections in blow-up/quenching rates are notoriously difficult to rigorously establish and numerically verify, as for instance was discussed in [13].

In this example, the solution u is minimum at two distinct points located on the horizontal axis and symmetrically about the origin, as shown in Fig. 14(a-b). The touchdown point $(x_{1c}, x_{2c}) \sim (0.57, 0.0)$ is isolated for comparison with the self-similar profile $\bar{v}_1(r)$. The contours of the solution are seen to approach circles as $(x_1, x_2) \to (x_{1c}, x_{2c})$, as shown in Fig. 14(c). This suggests the limiting profile near touchdown is radially symmetric. Indeed, good agreement is observed between $\bar{v}_1(r)$ and the numerical solution (*c.f.* Fig. 14(d)). A refined numerical study of the dynamics of (2) very close to the singularity would be necessary to confirm the self-similar nature of the touchdown profile. However, this is beyond the scope of the present work and of the numerical method employed in this article.

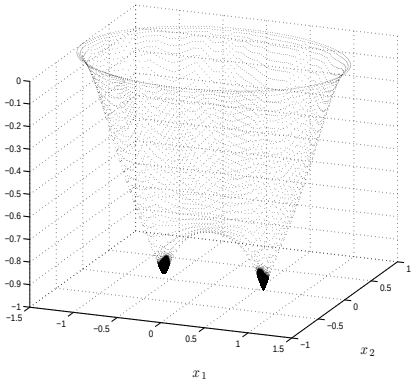

(a) Profile of numerical solution at touchdown.

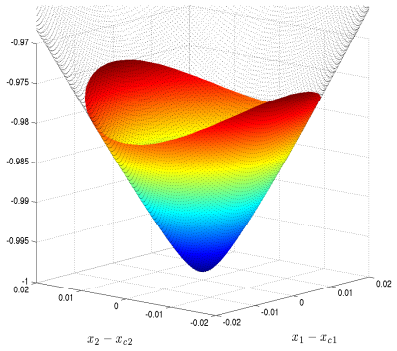

(b) Enlargement of (a) around $(0.57, 0.0)$ with interpolation on a polar grid centered at the touchdown point.

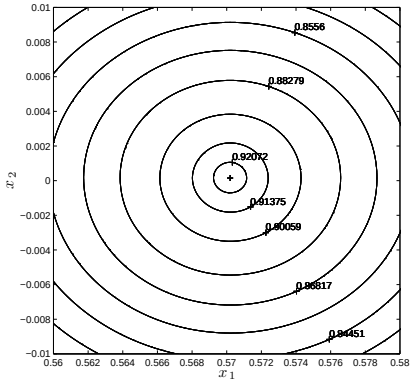

(c) Contours of the solution around the touchdown point with values of σ overlaid.

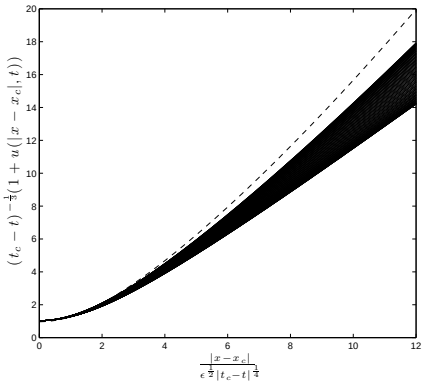

(d) Comparison of asymptotic profile $\bar{v}_1(\eta)$ (dashed) with the numerical solution along 100 radial cross-sections, equally spaced in the angular direction.

Figure 14: Comparison of asymptotic predictions with full numerics of (2) with $\varepsilon = 0.05$ on the ellipse. In Fig. 14(a), the numerical solution of (2) for $t_c - t = 9.357e^{-10}$ is shown with refinement in regions where $1 + u(x,t)$ is close to 0. In Fig. 14(b), an enlargement of the solution profile in the vicinity of the touchdown point is shown. The minimum is attained at $(x_{1c}, x_{2c}) = (0.5702, 0.0002)$ with a corresponding value $u(x_{c1}, x_{c2}) = -0.999$. Fig. 14(c) shows the contours of the solution in the vicinity of the touchdown point with the ratio of major to minor axis for the best-fit ellipse (*c.f.* [10]) overlaid. This ratio appears to be approaching 1 as $(x_1, x_2) \to (x_{1c}, x_{2c})$ indicating that solutions are represented by a radially symmetric function close to touchdown. In Fig. 14(d), solution profiles (solid) taken radially through the touchdown point are compared with the stable radially symmetric self similar profile $\bar{v}_1(\eta)$ (dashed) satisfying (34). Good agreement is observed.

6. Conclusions

In the present work, we have investigated the formation of singularities in a fourth order nonlinear parabolic partial differential equation in two-dimensions. We have shown that an asymptotic description of small time solutions provides a framework for establishing qualitative and quantitative predictions of the touchdown set based on two structures, $\omega(t_c(\varepsilon))$ and $\mathcal{S}$. The efficacy of the predictive ability of this framework was demonstrated on a wide variety of domains and found to be very good, particularly for ε small.

One of the main conclusions of this work is that the leading order approximation of the solution profile reaches a local minimum either at a discrete set of points or on a one dimensional curve $\omega(t)$. In the absence of noise, touchdown would thus occur simultaneously at a finite number of points on $\mathcal{S}$ or everywhere on $\omega(t_c(\varepsilon))$. Curvature effects however favour touchdown at points on $\omega(t_c(\varepsilon))$ of highest curvature. Noise typically leads to the selection of one of the points on $\omega(t_c(\varepsilon))$ as the touchdown location. Moreover, an instability along $\omega(t)$ also culminates in touchdown at a single point on $\omega(t_c(\varepsilon))$. The various examples discussed in this paper were chosen to illustrate how the above effects combine or compete to select the touchdown location. The numerical simulations confirm the robustness of our approach and the predictive power of the leading order theory discussed in this article.

As a nonlinear PDE, equation (2) has very rich dynamics, since touchdown may result from the combination of an instability along $\omega(t)$ and the effect of a singular nonlinearity. This phenomenon is interesting in its own right and deserves further study in a separate line of work. It is also likely that the multiple touchdown phenomenon discussed in this article is a generic feature of fourth order PDEs which form singularities in finite time. The theory developed in the present work should therefore be applicable to equations with more general nonlinearities.

At the level of applications, the theory developed herein may have several ramifications for the design of MEMS devices. The most relevant feature is that touchdown may occur simultaneously at several points throughout the domain and that these touchdown locations can be parameterized through the applied voltage. This phenomenon may allow the life of MEMS devices to be extended by spreading the wear out over the extent of the device. Additionally, the potato example shows that it is possible for the touchdown location to switch abruptly from one point to another in Ω as ε is varied. More exotic MEMS devices could thus be built by extending these ideas to other types of domains. An interesting inverse problem would be to construct regions Ω for a given touchdown set $\tau_d(\Omega)$.

Acknowledgments

We thank Jeff Hyman and Dr. C. L. Winter for the generous use of their computing resources.

References

[1] J. A. Pelesko, D. H. Bernstein, *Modeling MEMS and NEMS*, Chapman Hall and CRC Press, (2002).

[2] G. Flores, G. Mercado, J. A. Pelesko and N. Smyth, *Analysis of the Dynamics and Touchdown in a Model of Electrostatic Mems*, SIAM Journal on Applied Mathematics Vol. 67, No. 2 (2006), pp. 434-446.

[3] J. A. Pelesko, *Mathematical Modeling of Electrostatic MEMS with Tailored Dielectric Properties*, SIAM Journal on Applied Mathematics (2002), Vol. 62, No. 3, pp. 888-908.

[4] N. D. Brubaker, J. A. Pelesko, *Non-linear effects on canonical MEMS models*, European Journal of Applied Mathematics (2011) 22 : pp 455-470

[5] Arnold, Douglas N, Falk, Richard S, Gopalakrishnan, Jay. *Mixed finite element approximation of the vector Laplacian with Dirichlet boundary conditions.* Submitted.

[28] C.J. Budd, J. F. Williams, *How to adaptively resolve evolutionary singularities in differential equations with symmetry*, J. Engineering Mathematics, 66 (2010), no 3, 217–236.

[7] Ciarlet, Philippe G, Raviart, Pierre–Arnaud. *A mixed finite element method for the biharmonic equation.* Mathematical aspects of finite elements in partial differential equations (Proc. Sympos., Math. Res. Center, Univ. Wisconsin, Madison, Wis., 1974), pp. 125-145.

[8] Ishihara, Kazuo, *A Mixed Finite Element Method for the Biharmonic Eigenvalue Problems of Plate Bending.* Publ. RIMS, Kyoto Univ.14 (1978), 399-414.

[9] Miyoshi, T., *A finite element method for the solutions of fourth order partial differential equations*, Kumamoto J. Sci. (Math.), 9 (1972), 87-116.

[10] Andrew W. Fitzgibbon, Maurizio Pilu, and Robert B. Fisher, *Direct least-squares fitting of ellipses*, IEEE Transactions on Pattern Analysis and Machine Intelligence, 21(5), 476–480 (1999).

[11] Z. Guo, J. Wei, *Entire Solutions and Global Bifurcations for a Biharmonic Equation with Singular Nonlinearity in* $\mathbb{R}^3$, Advances Diff. Equations, **13**, (2008), No. 7-8, pp. 743–780.

[12] Z. Guo, J. Wei, *On a Fourth Order Nonlinear Elliptic Equation with Negative Exponent*, SIAM J. Math. Anal., **40**, No. 5, (2009), pp. 2034–2054.

[13] A.E. Lindsay, J. Lega, *Multiple Quenching Solutions of a Fourth Order Parabolic PDE with a singular nonlinearity modelling a MEMS Capacitor*, SIAM J. Appl. Math. (2012), 72(3), 935-958.

[14] C.J. Budd, V.A. Galaktionov and J. F. Williams, *Self-Similar Blow-up in Higher-Order Semilinear Parabolic Equations*, SIAM J. Appl. Math, Vol. 64 No.5, pp. 1775-1809 (2004).

[15] Y. Guo, *Dynamical solutions of singular wave equations modeling electrostatic MEMS*, SIAM, J. Appl. Dynamical Systems, 9 (2010), 1135–1163.

[16] Y. Guo, *On the partial differential equations of electrostatic MEMS devices III: refined touchdown behavior*, J. Diff. Eqns. 244 (2008), 2277-2309.

[17] Fanghua Lin and Yisong Yang, *Nonlinear non-local elliptic equation modelling electrostatic actuation*, Proc. R. Soc. A (2007) **463**, 1323-1337.

[18] A. E. Lindsay, M. J. Ward, *Asymptotics of Some Nonlinear Eigenvalue Problems for a MEMS Capacitor: Part I: Fold Point Asymptotics*, Methods Appl. Anal., **15**, No. 3, (2008), pp. 297–325.

[19] A. E. Lindsay, M. J. Ward, *Asymptotics of some nonlinear eigenvalue problems for a MEMS capacitor: Part II: Singular Asymptotics*, Euro. Jnl of Applied Mathematics (2011), vol. 22, pp. 83-123.

[20] Y. Guo, Z. Pan, M. J. Ward, *Touchdown and Pull-In Voltage Behaviour of a MEMS Device with Varying Dielectric Properties*, SIAM J. Appl. Math., **66**, No. 1, (2005), pp. 309–338.

[21] A.J.Bernoff and T.P. Witelski, *Stability and dynamics of self-similarity in evolution equations*, Journal of Engineering Mathematics, vol. 66 no. 1-3 (2010), pp. 11-31.

[22] A.J.Bernoff and T.P. Witelski, *Dynamics of three-dimensional thin film rupture*, Physica D, 147 (2000), pp. 155-176.

[23] Andrew J. Bernoff, Andrea L. Bertozzi and Thomas P. Witelski, *Axisymmetric surface diffusion: Dynamics and stability of self-similar pinch-off*, J. Stat. Phys. (1998) 93, 725-776.

[24] A.J.Bernoff and T.P. Witelski, *Stability of self-similar solutions for van der Waals driven thin film rupture*, Physics of Fluids, Vol.11 No. 9 (1999).

[25] V.A. Galaktionov and J. F. Williams, *Blow-up in a fourth-order semilinear parabolic equation from explosion-convection theory*, Euro. Jnl Applied Mathematics (2003), vol. 14. pp 745-764.

[26] V.A. Galaktionov, *Five types of blow-up in a semilinear fourth-order reaction-diffusion equation: an analytical-numerical approach*, (2009) Nonlinearity **22** 1695-1741.

[27] M. C. Kropinski, A. E. Lindsay, M. J. Ward (2011), *Asymptotic Analysis of Localized Solutions to Some Linear and Nonlinear Biharmonic Eigenvalue Problems*, Studies in Applied Mathematics, 126: no. doi: 10.1111/j.1467-9590.2010.00507.x.

[28] C.J. Budd, J. F. Williams, *How to adaptively resolve evolutionary singularities in differential equations with symmetry*, J. Engineering Mathematics, 66 (2010), no 3, 217–236.